Supplementary Data

All-Carbon Patterning of HOPG on the Nanometer Scale with non-IPR Fullerenes

Artur Böttcher[a], Stefan-Sven Jester[b], Daniel Löffler[a], Johannes Seibel[a] and Manfred M. Kappes[a,c]

[a]Institute of Physical Chemistry, Karlsruhe Institute of Technology, Kaiserstraße 12, 76131 Karlsruhe, Germany;

[b]Kekulé-Institut für Organische Chemie und Biochemie, Rheinische Friedrich-Wilhelms-Universität Bonn, Gerhard-Domagk-Str. 1, 53121 Bonn, Germany;

[c]Institute of Nanotechnology, Karlsruhe Institute of Technology, Kaiserstraße 12, 76131 Karlsruhe, Germany.

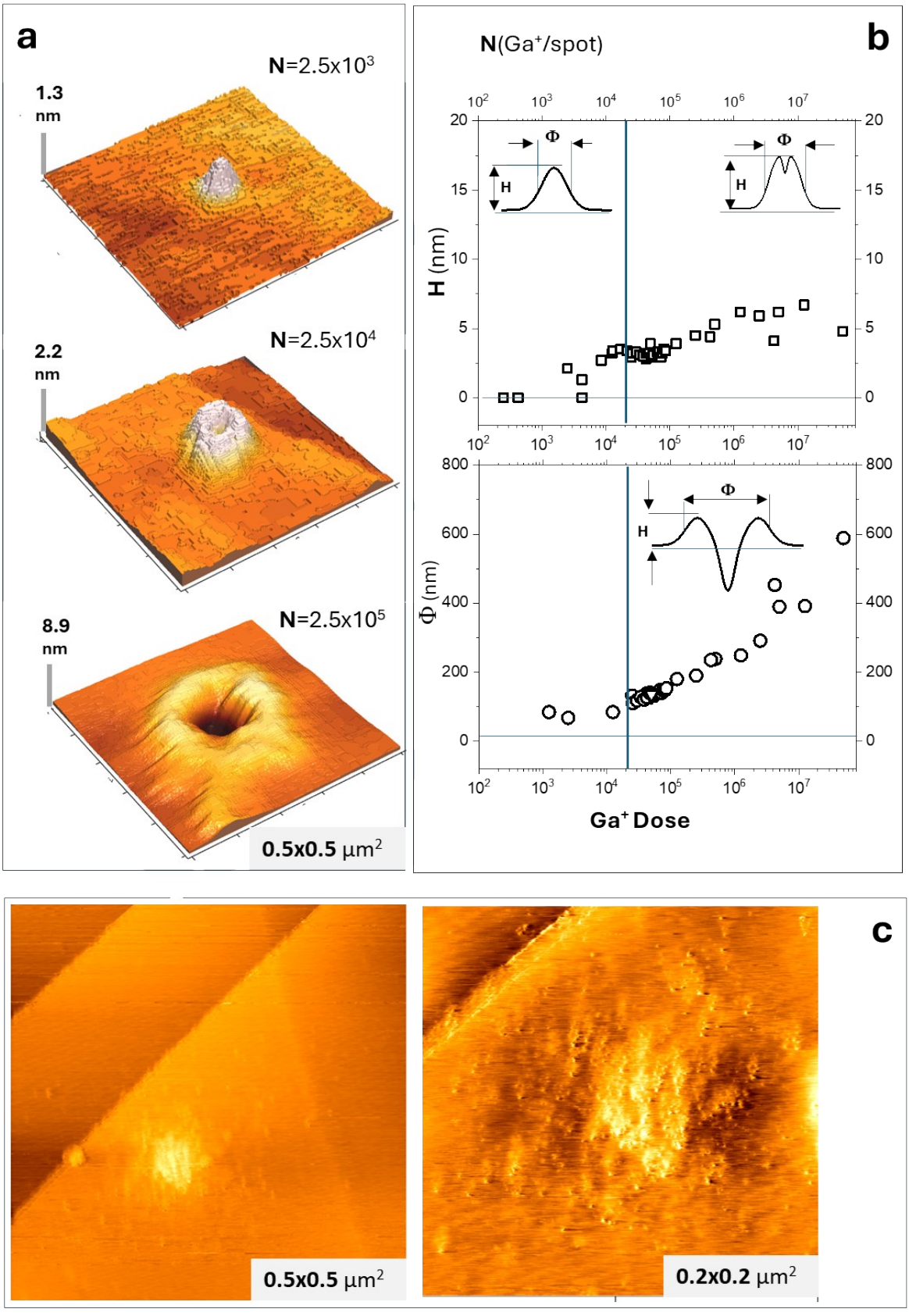

Fig. S1: AFM (**A**) and STM (**C**) images illustrating the morphology of amorphous carbon spots created by the interaction of the focused Ga^+ beam (30 keV) with the HOPG basal plane. Panel **A** shows the ion dose dependency of the spot profiles: increasing ion dose from 10^3 to 10^5 Ga^+/spot changes the defect form from small, bell-shaped hillocks to volcano-like protrusions with a large crater in the center. For doses <10^4 Ga^+/spot the mean height of the hillocks drops below 2 nm and their characteristic diameter

(full width at half maximum, FWHM) is ~100 nm. For N<10^4 Ga^+ ions, hillocks with bell-like shapes were observed. For larger Ga^+ doses volcano-like profiles with a crater in the center grow in width and depth. The STM images in panel C show that low-amplitude topographic "halos" (extending beyond ϕ) form about some spots, e.g. due to redeposition of ejected material or backscattering of C atoms from the collision cascade. This is reflected by the bright dot-shaped features adjacent to the main FIB impact region in the STM image (imaging conditions: U_{tip}= +50 mV, I=1 nA). These halos may contribute to the effective capture cross-section for diffusing C_{58}.

We performed TRIM calculations for low ion dose of N=2.5x10^3 ions/dot.[1] The results evidence lateral extension of the amorphous dots of~80 nm, which fits well to the profiles measured for low dose patterning, <10^4 ions/dot. The simulations are based on the assumption of local amorphization of graphene stacks as the main defecting process.[2] Panel **B** shows three groups of elevation profiles we found experimentally by AFM when increasing the Ga^+ dose in the range 10^3-10^7. For all profiles we measured the height H and the lateral extension ϕ (diameter) as explained by the schemes in panel B. The width and height of the hillock profiles are plotted as functions of the Ga^+ dose (panel B). The elevation profiles of single hillocks change considerably with increasing Ga^+ dose: for doses <10^4 ions/dot narrow single bell-like profiles are observed. For moderate doses, 10^4-10^5 ions/dot, small holes start to be drilled in the bell-like profiles (the vertical lines in panel B mark the dose where the formation of craters sets on). All hillocks created by applying ion doses >10^5 ions/dot exhibit wide volcano-like profiles with deep craters in the center (see the lower plot in panel B). Our analysis of the hillock profiles fits well with the data published by B.S. Archanjo et al. [3]

All our C_{58} deposition experiments were performed using defect arrays prepared in the low dose regime, N<10^4, which provides bell like spots with heights of 1-2 nm and lateral extensions around ϕ ~100 nm (panel **B** and **C**). This choice is supported by the range of the mean free gliding length Λ which is estimated to be around 300 nm and consequently enables to study the surface diffusion mediated island growth. Note also, that Ga^+ implantation leads to deep subsurface deposition of (chemically inert) gallium atoms which we assume do not influence C_{58} island growth.

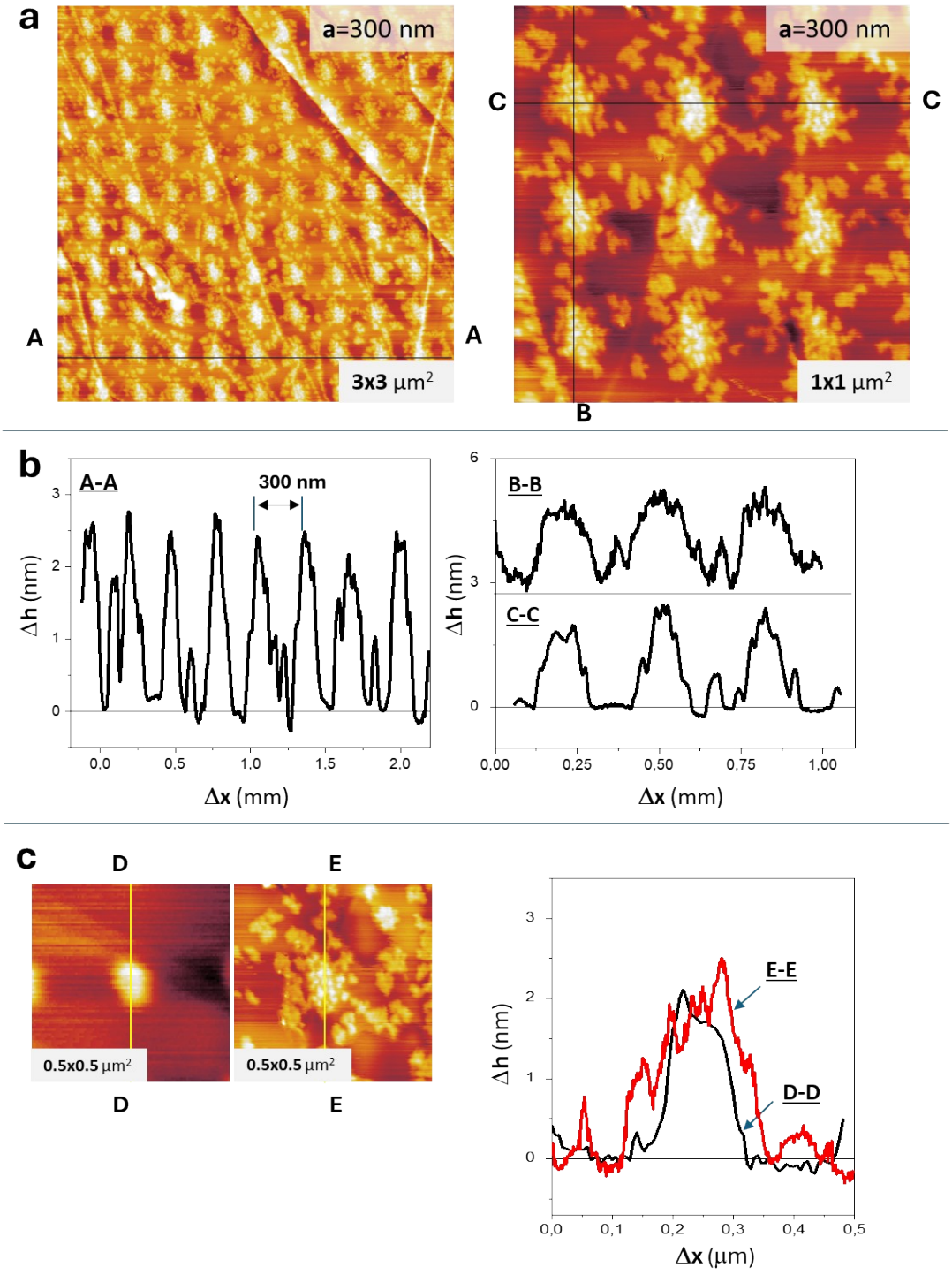

Fig. S2: AFM images and line scans for a C_{58}/FIB/HOPG surface to illustrate the nominal height of FIB structured amorphous carbon pinning sites versus the height of C_{58}-derived islands as generated by ion deposition onto FIB defect arrays and subsequent thermal annealing. (**a**) 3 × 3 µm² and 1 × 1 µm² images of the same sample, (**b**) corresponding line scans, (**c**) high resolution 0.5 × 0.5 µm² image of an as-generated FIB defect and of a FIB defect on the same substrate after C_{58} decoration and corresponding line scans. The line scans indicate that the mean height of the pinning sites remains about the same after C_{58} decoration – ca. 2 nm. This suggests that island growth takes place preferentially by attachment of mobile cages to the *rims* of dendritic islands (via intercage bridges, -2AP-2AP-). (FIB: I=10 pA, t=0.4 ms, D^+= 2.5 × 10^4 Ion/spot, *a* = 300 nm; LECBD: E_0 = 6 eV, Q = 1 ML C_{58}, annealing A[10'/550K]).

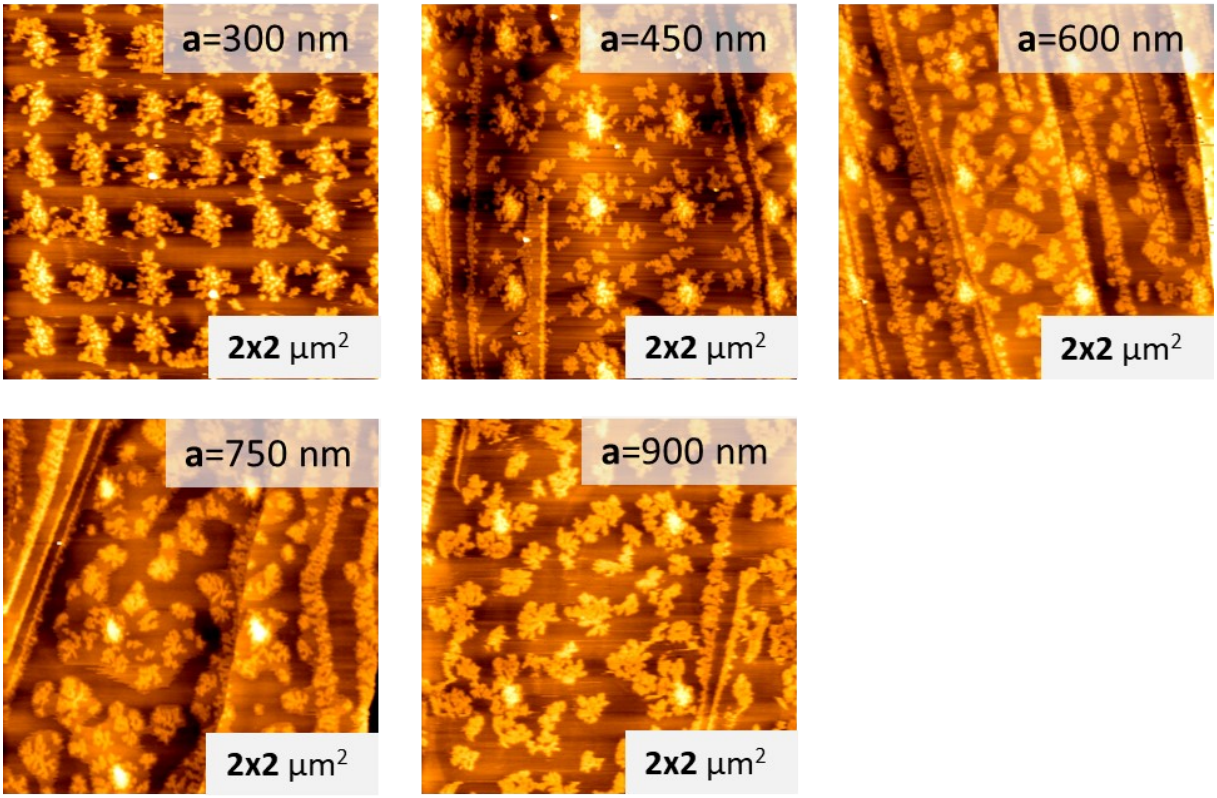

Fig. S3: Typical AFM images (2 × 2 µm^2) for C_{58}/FIB/HOPG surfaces obtained after C_{58} deposition followed by *ten* minute in-situ annealing at 550 K - using five arrays differing in their lattice constants: a = 300, 450, 600, 750 and 900 nm. These images were used to evaluate island coverages as indicated in figure 3(c) main text. Best decoration quality ratio under the conditions used is obtained for a 300 nm period array (FIB: I = 10 pA, t = 0.4 ms, $D^+ = 2.5 \times 10^4$ Ions/spot, a = 300-900 nm; LECBD: $E_0 = 6$ eV, Q = 1 ML C_{58}, A[10'/550K]). This series illustrates the competition between the "natural" defects in the HOPG surface (predominantly step edges) and the FIB written defects. Both types of "defects" can act as pinning sites. When the distance between adjacent FIB defects, a, becomes shorter than the mean gliding length of sticking C_{58} cages on wide terraces, Λ, pinning is governed nearly exclusively by the FIB defects.

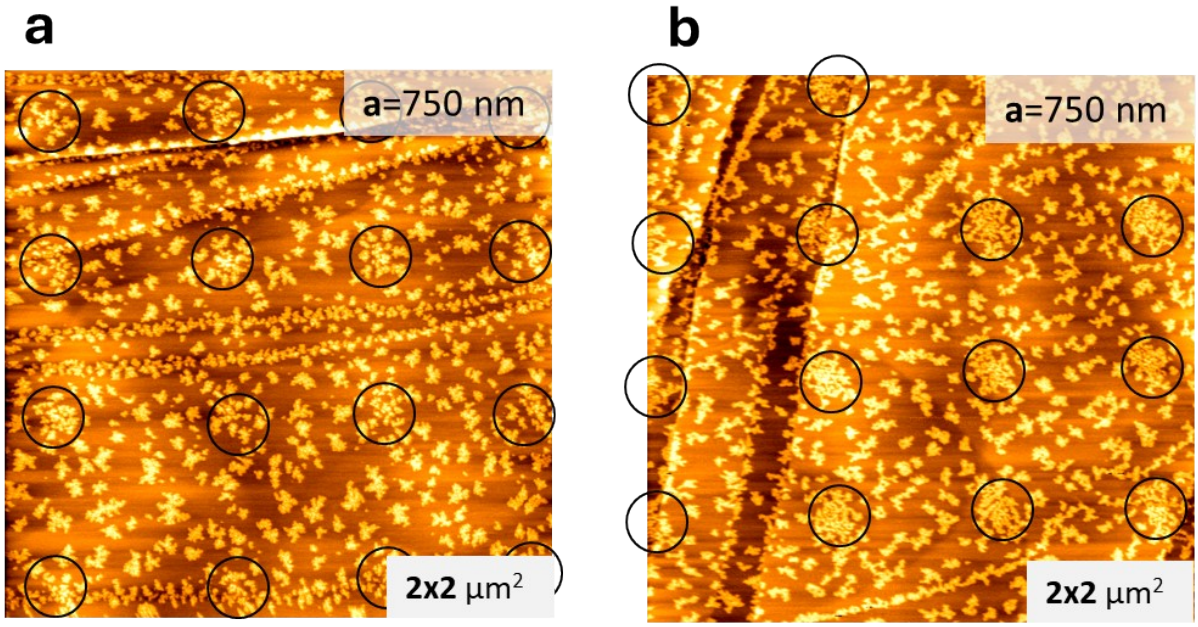

Fig. S4: Typical AFM images (3 × 3 µm^2) for two separate C_{58}/FIB/HOPG samples both with 750 nm defect lattice constant: (**a**) after room temperature C_{58} deposition (followed directly by transfer to an ex-situ AFM without a thermal annealing step) and (**b**) after an intermediate thermal annealing step in which the sample was heated to 550 K for five minutes. The black circles are meant to guide the eye. Heating enhances the accumulation of C_{58} cages about the defect arrays. (Patterning conditions → FIB: I = 10 pA, t = 0.4 ms, $D^+ = 2.5 \times 10^4$ Ions/spot, *a* = 750 nm; LECBD: $E_0 = 6$ eV, Q = 1 ML C_{58}, A[5'/550K]).

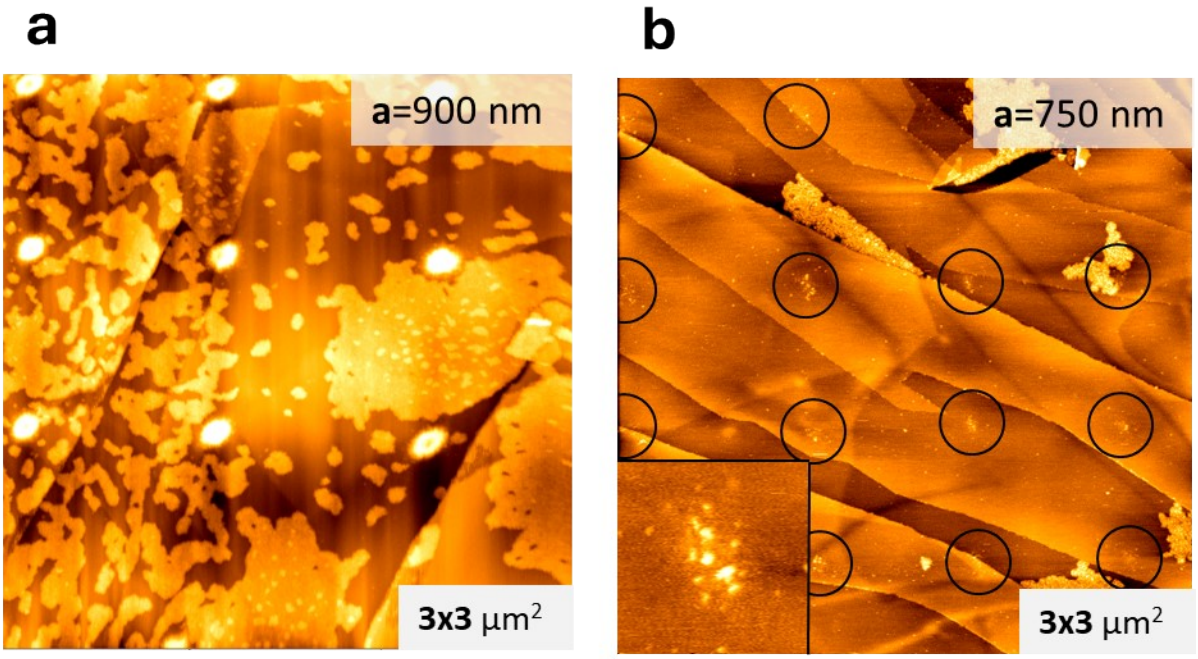

Fig. S5: a) AFM image (3x3 µm^2) taken after deposition of a submonolayer of C_{60} onto a Ga^+-FIB patterned HOPG surface (2D array with lattice constant of 900 nm) followed by thermal annealing. The resulting surface is decorated by large compact islands terminated by smooth rims (in contrast to equivalently generated C_{58} island films which are dendritic in nature, see e.g. Fig. S3). It appears that C_{60} islands are growing independently of the FIB dots (white spots), i.e. their pinning role is not recognizable. The smooth island rims reflect thermally activated surface diffusion of van der Waals interacting C_{60} cages – which only become stabilized at threefold and higher coordinated rim sites (FIB: I=10 pA, t=0.4 ms, D^+= 5.5x10^4 Ion/spot, *a*=900 nm; LECBD: E_0= 6 eV, Q=3 ML C_{60}; A[5'/500K). **b**) AFM image (3x3 µm^2) of a C_{60}/FIB/HOPG surface with 750 nm lattice constant defect array after soft-landing C_{60} at room temperature under the same conditions as for C_{58} in figure S4(a), i.e. *no subsequent thermal annealing step* before AFM imaging. Note, that the surface is covered with large compact islands which are predominantly not associated with the FIB defects. On closer inspection, the amorphous carbon defects show a few protrusions attributable to direct sticking of C_{60}^+ incident from gas-phase. (FIB: I=10 pA, t=0.4 ms, D^+= 2.5x10^4 Ion/spot, *a*=750 nm; LECBD: E_0= 6 eV, Q=0.5 ML C_{60}; A[5',500K]).

References

[1] S.-S. Jester, Nanostrukturierte Kohlenstoffverbindungen, Dissertation, Karlsruhe Institut für Technologie, 2008. https://doi.org/10.5445/IR/1000009952.

[2] J.P. Biersack, L.G. Haggmark, A Monte Carlo computer program for the transport of energetic ions in amorphous targets, *Nuclear Instruments and Methods* **1980**, *174,* 257–269.

[3] B.S. Archanjo, I.O. Maciel, E.H. Martins Ferreira, S.B. Peripolli, J.C. Damasceno, C.A. Achete, A. Jorio, Ion beam nanopatterning and micro-Raman spectroscopy analysis on HOPG for testing FIB performances, *Ultramicroscopy* **2011,** *111*, 1338–1342.